RSC Advances

This is an *Accepted Manuscript*, which has been through the Royal Society of Chemistry peer review process and has been accepted for publication.

Accepted Manuscripts are published online shortly after acceptance, before technical editing, formatting and proof reading. Using this free service, authors can make their results available to the community, in citable form, before we publish the edited article. This *Accepted Manuscript* will be replaced by the edited, formatted and paginated article as soon as this is available.

You can find more information about *Accepted Manuscripts* in the Information for Authors.

Please note that technical editing may introduce minor changes to the text and/or graphics, which may alter content. The journal's standard Terms & Conditions and the Ethical guidelines still apply. In no event shall the Royal Society of Chemistry be held responsible for any errors or omissions in this *Accepted Manuscript* or any consequences arising from the use of any information it contains.

ROYAL SOCIETY OF CHEMISTRY

www.rsc.org/advances

Microstructure, electrical properties and temperature stability in $Bi_{0.5}Na_{0.5}Zr_{0.95}Ce_{0.05}O_3$ modified R-T phase boundary of potassium-sodium niobium lead-free ceramics

Zhi Tan, Jie Xing, Laiming Jiang, Lingguang Sun, Jiagang Wu, Wen Zhang, Dingquan Xiao and Jianguo Zhu*

Department of Materials Science, Sichuan University, Chengdu 610064, People's Republic of China

Submitted to

RSC Advances

RSC Advances Accepted Manuscript

*Author to whom correspondence should be addressed: E-mail: nic0400@scu.edu.cn

Abstract

(1-*x*)$K_{0.48}Na_{0.52}Nb_{0.95}Sb_{0.05}O_3$-*x*$Bi_{0.5}Na_{0.5}Zr_{0.95}Ce_{0.05}O_3$ [(1-*x*)KNNS-*x*BNZC] lead-free piezoelectric ceramics, with doping ratio of *x* ranging from 0 to 0.05, have been synthesized by the conventional solid state sintering method. The phase transition behavior, microstructure as well as piezoelectric properties of (1-*x*)KNNS-*x*BNZC ceramics were systematically investigated using XRD, SEM, and other devices with different doping amount of BNZC. It was found that the piezoelectric properties of (1-*x*)KNNS-*x*BNZC ceramics were improved obviously with the proper doping amount of addition, $0.03< x <0.04$, due to the coexistence of rhombohedral and tetragonal phases in the ceramics near room temperature. The piezoelectric constant d_{33} of the ceramics first increases and then decreases with the increasing of the doping amount. A remarkably strong piezoelectricity has been obtained in the ceramics with a peak d_{33} value of ~441 pC/N. The excellent piezoelectric properties of (1-*x*)KNNS-*x*BNZC ceramics with x=0.034 are obtained: d_{33}~441 pC/N, k_p~0.44, Q_m~31, ε_r~2447, tanδ~0.037, T_C~215℃, P_r~15.7 μC/cm^2, E_C~8.2 kV/cm, respectively. With the annealing temperature reaching 250℃, the d_{33} values of the ceramics are still greater than 330 pC/N, which present a good temperature stability of piezoelectricity. It was believed that such a material system is a very promising candidate for lead-free piezoelectric ceramics.

RSC Advances Accepted Manuscript

1. Introduction

Lead-based piezoelectric ceramics, such as PZT, PMN-PT, have been widely used in various field as actuators, sensors and transducers due to their excellent piezoelectric properties.[1,2] However, high lead content of lead-based piezoelectric ceramics, which is more than 60%, causes the environment issues during the whole product life period, including ceramics' preparation, processing, and even disposal.[3-6] Therefore, much attention has been paid to the replacement of lead-based materials by the lead-free piezoelectric materials in electronic products. Intensive research has focused on several lead free candidate materials such as $BaTiO_3$, $Bi_{0.5}Na_{0.5}TiO_3$ and $K_{0.5}Na_{0.5}NbO_3$ (abbr. as BT, BNT and KNN). In the last decade, KNN-based ceramics is special concerned in lead-free materials because of large piezoelectric response, strong ferroelectricity and high Curie temperature.[3-5,7]

In the past research, constructing the boundaries of coexistence phases has been used as one of the most effective ways to enhance piezoelectric properties of KNN-based ceramics, such as orthorhombic-tetragonal (O-T) phases and rhombohedral-orthorhombic (R-O) phases coexistence.[4,5,8-13] Two phase boundaries are constructed in KNN-based ceramics at room temperature by enhancing the R-O phase transition point to room temperature or reducing the O-T phase transition point. Researchers have gotten great achievement in KNN-based ceramics on phase boundary, where presents larger piezoelectric properties with more polarization orientation on phase boundary.[5] After these work, R Zuo and W Liang make a point that rhombohedral-tetragonal (R-T) boundary is constructed in KNN-based ceramics by shifting $T_{R\text{-}O}$ and $T_{O\text{-}T}$ to room temperature, respectively.[14,15] Excellent piezoelectric constant (d_{33}~380pC/N and 344pC/N, respectively) proved that constructed R-T boundary is a feasible method for enhancing piezoelectric properties in KNN-based ceramics.[14,15]

In previous report, both Sb^{5+} and $Bi_{0.5}Na_{0.5}ZrO_3$ were used to increase $T_{R\text{-}O}$ and decrease $T_{O\text{-}T}$, respectively.[5,16-19] On the other hand, CeO_2 is often used as a donor dopant or additive for the lead-based piezoelectric ceramics to improve their electrical properties.[20] It has also reported that Ce-doping could improve dielectric and piezoelectric properties in KNN-based ceramics.[21] In this work, Zr element of $Bi_{0.5}Na_{0.5}ZrO_3$ was replaced by a small amount of Ce to form a new doping component $Bi_{0.5}Na_{0.5}Zr_{0.95}Ce_{0.05}O_3$. The ceramics with a series of compositions $(1\text{-}x)K_{0.48}Na_{0.52}Nb_{0.95}Sb_{0.05}O_3\text{-}xBi_{0.5}Na_{0.5}Zr_{0.95}Ce_{0.05}O_3$ [(1-x)KNNS-xBNZC] were synthesized by a conventional solid-state sintering method. It was found that the R-T boundary had been constructed in (1-x)KNNS-xBNZC ceramics at room temperature when $0.03<x<0.04$. A large d_{33} of 441 pC/N have

RSC Advances Accepted Manuscript

been obtained for the ceramics with x=0.034, it is larger than that of Saito *et al*. reported (d_{33}~416 pC/N).[7] Finally, the ceramics of phase structures, microstructures, piezoelectric，ferroelectric and dielectric properties and thermal stability of (1-x)KNNS-xBNZC ceramics were investigated and discussed.

2.Experimental procedure

In this work, (1-x)$K_{0.48}Na_{0.52}Nb_{0.95}Sb_{0.05}O_3$-$xBi_{0.5}Na_{0.5}Zr_{0.95}Ce_{0.05}O_3$ [(1-x)KNNS-xBNZC] ceramics were prepared by conventional solid state sintering method. Na_2CO_3 (99.8%), Nb_2O_5 (99.5%), Bi_2O_3 (99.999%), K_2O_3 (99%), Sb_2O_3 (99.99%), ZrO_2 (99%), and CeO_2 (99.99%) were used as raw powders, weighed according to stoichiometric ratio of the ceramics. The powders were mixed by ball-milling in ethanol for 12h, then dried and calcined at 850 ℃ for 6h. The dried powders were mixed with poly vinyl alcohol (PVA, 8%) and pressed into discs with diameter of 10mm and thickness of 1mm under 10 MPa. After burning out the PVA, the pellets were sintered at a temperature range of 1070~1140℃ for 3h in air. Sliver paste electrodes were coated on both sides of pellets and fried at 700 ℃ for 10 min. These ceramics were poled in silicon oil under a DC electric field of 2~4 kV/mm for 10~30 min from room temperature to 60 ℃, and all the piezoelectric properties of the samples were measured after the poling for 24h.

The structural properties of the samples were investigated by X-ray diffraction (XRD) (DX 2700, Dandong, China). The surface morphologies were characterized by the filed mission-scanning electron microscopy (FE-SEM, JSM7500, Japan). The curves of dielectric constant (ε_r) against temperatures of the sintered samples were measured using an LCR analyzer (HP 4980, Agilent, U.S.A. and TH2816A). Polarization verse electric field (P-E) hysteresis loops of the ceramics were conducted at 10 Hz using a Radiant Precision Work-station (USA).Their piezoelectric constant d_{33} and electromechanical coupling factor k_p was characterized by a Belincourt meter (ZJ-3A, Institute of Acoustics, Chinese Academy of Sciences, China) and an impedance analyzer (HP 4294A, Agilent, U.S.A.) according to the IEEE standards.

3.Results and discussion

Figure 1(a) show the XRD patterns of the (1-x)KNNS-xBNZC ceramics. From Fig.1(a), it was

RSC Advances Accepted Manuscript

found that all the ceramics form a pure perovskite phase, which presents the formation of a stable solid solution. Figure 1(b) gives the enlarged XRD patterns of the ceramics with measuring range 44~47°. The ceramics present orthorhombic phase when x is less than 0.01. With the doping content of BNZC increasing, a broad and split peak has been observed at the composition of x=0.02 in Figure 1(b). The coexistence of the rhombohedral phase, orthorhombic phase and tetragonal phase is considered in the ceramics according to the two close dielectric peaks in Figure 2(b), which implied the coexistence of three phases). So the XRD pattern of the ceramics was simulated using Lorentz function, as shown in Figure 1(c). The result consists with our prediction. For $0.03 \leq x \leq 0.04$, the coexistence of the rhombohedral phase and tetragonal phase appears, which are confirmed by Figure 1(d) and Figure 2(c)-(e). At the same time, the ceramics with x=0.05 show a single peak in Figure 2(b). The ceramics are considered as R phase because of the P-E loop and non-zero value of d_{33} [Figure 5(a) and Figure 6(a)]. We also calculated their crystal parameters, showing $a=b=c$=3.9859Å and $\alpha=\beta=\gamma$=89.9878°. The results further indicated the ceramics with x=0.05 is R phase.

The temperature-dependence dielectric constant (ε_r) of the ceramics from -120℃ to 200℃ were characterized to investigate the influence of doping BNZC on the phase transition of KNN-based ceramics, as shown in Figure 2. Two phase transition peaks at $T_{R\text{-}O}$ and $T_{O\text{-}T}$ could be found in the ceramics with x=0 and 0.02. The phase transition peaks at $T_{O\text{-}T}$ gradually decreases and $T_{R\text{-}O}$ gradually increases with x from 0 to 0.04, which means $T_{R\text{-}O}$ and $T_{O\text{-}T}$ gradually approach with x increasing. Eventually, as shown in the Figure 2(c) to 2(e), the two peaks mixed together and became one peak. Considering both XRD patterns and ε_r versus T curves in Figures 1 and 2, the R-T phase boundary had been constructed successfully in the ceramics at room temperature when x in the range of 0.03 to 0.04. However, the R-T phase boundary is restrained with further increased of BNZC content (x=0.05), as shown in Figure 2(f). At the same time, Figure 2(f) shown a diffused Curie peak (Curie temperature-T_C) because of the dramatic decrease in grain size [see Figure 4(d)].

For further study of the BNZC content on T_C and the phase evolution, the temperature dependent dielectric constant (ε_r) of the (1-x)KNNS-xBNZC ceramics was measured at 100 kHz in the temperature range of 30–450℃, as shown in Figure 3(a). The T_C presents the tendency of decreasing gradually with x increasing. And the curves is comparatively flat when x=0.05, which indicated that the T_C is diffused. According to the research results of Figure 2(a)-(f) and Figure 3(a), the phase diagram was drawn to show T_C, $T_{O\text{-}T}$ and $T_{R\text{-}O}$ of the (1-x)KNNS-xBNZC ceramics as function of BNZC [Figure

RSC Advances Accepted Manuscript

3(b)]. It clearly shows T_C, T_{O-T} and T_{R-O} of the (1-x)KNNS-xBNZC ceramics change as the x. It was could found that R-T phase boundary was formed at room temperature in the (1-x)KNNS-xBNZC ceramics with $0.03 \leq x \leq 0.04$.

To identify the evolution of microstructures of the ceramics, their micrographs were investigated. Figure 4(a)-4(d) show the SEM surface micrographs of the ceramics with x=0, 0.02, 0.034, and 0.05, respectively. It was found that the grain size gradually increases with increasing BNZC content when x is less than 0.034, and then drops dramatically with further increasing BNZC content (x=0.05). In addition, the ceramics with $x \leq 0.034$ show a nonuniform grain sizes. Small grains exists in grain boundaries and distributed around the large ones. It is probably caused by the following reasons: (I) For low BNZC contents, the liquid phase formed due to Bi element has lower melting point in sintering process, which could promote the grain growth of the ceramics, giving rise to the increase in grain size.[22] (II) For higher BNZC contents, excess BNZC gather at grain boundary, and Zr, Ce can prohibit the grain growth during sintering process, resulting the grain size decreases significantly to less than 1μm, as shown in Figure 4(d).[21,23]

The ferroelectric switching behavior of the ceramics was studied in terms of their P-E loops. Figure 5(a) shows the P-E curves of the ceramics as x increases from 0 to 0.05, and they were measured at room temperature and 10 Hz. All the ceramics have a typical P-E loop except for the one with x=0.05, because the ceramics with x=0.05 involve the rhombohedral phase.[14] For the study of ferroelectric properties in detail as a function of x, remanent polarization (P_r) and coercive field (E_C) were derived from P-E loops of Figure5(a),as shown in Figure5(b). From Fig.5, it was found that the P_r of the ceramics present the tendency of firstly increases and then decreases with the increasing of x. After the appearing the maximum of P_r at x=0.01, the P_r gradually drops with further increasing BNZC content. And E_C presents downtrend on the whole as BNZC content increases, but it shows abnormal fluctuations in composition range of x=0.03-0.04, which just at R-T phase boundary.

Figure 6(a) shows the variations of d_{33}, planar coupling factor (k_p) and mechanical quality factor (Q_m) versus x of the ceramics, measured at room temperature after 24 hours of polarization. From Fig.6(a), it was found that the d_{33} of the ceramics clearly increases as x changes from 0 to 0.034 and then drops quickly as x further increasing. The k_p of the ceramics shows the trend of first increases and then gradually decreases with increasing x, while the Q_m of the ceramics first decreases and then increases as x changes from 0 to 0.04, whose minimum is 31 at x=0.034.

RSC Advances Accepted Manuscript

The dielectric constant (ε_r) and dielectric loss (tanδ) of the ceramics with different BNZC contents are shown in Figure 6(b). The ε_r increases as x increases, reaching maximum with x=0.036, and then decreases with further increasing x. In addition to x=0.05, the trend of tanδ is just opposite as compare with ε_r, and it has a lower value (tanδ~0.036-0.038) when x=0.03-0.038. In this work, d_{33} reaches a maximum value of ~441 pC/N for x=0.034 (k_p~0.44, Q_m~31, ε_r~2447, tanδ~0.037, T_C~215℃, P_r~15.7μC/cm^2, E_C~0.82kV/mm), which is larger than those of most others reported, as shown in Table 1, the piezoelectric properties and Curie temperature T_C of some typical KNN-based lead-free ceramics with large d_{33} were listed. Moreover, the large piezoelectric constant of the ceramics in this work is almost comparable to some lead-based piezoelectric ceramics, such as PZT4.[28]

The ceramics with large d_{33} have three important factors, (I) Doping BNZC makes T_{O-T} gradually decrease and T_{R-O} gradually increases, and then the ceramics form R-T phases coexistence at room temperature when x in the range of 0.03 to 0.04. The formation of the R-T phase coexistence is responsible for such a large d_{33} value of this work.[14,15,24-26,33] (II) It was reported that d_{33} is proportional to $\varepsilon_r P_r$ in piezoelectric ceramics. Larger ε_r were obtained in the ceramics with 0.03<x<0.04 [Figure 6(b)], Which leads to an enhanced piezoelectric properties.[26-28] (III) It is well known that the increased grain sizes result in the enhance piezoelectric properties, because the smaller grain sizes are in favor of the reduction in the number of domain variants.[29-32] Figure 4(c) shows giant grain sizes when x=0.034. In addition, the poor d_{33} of the ceramics with x=0.05 is partly attributed to the low and diffused Curie peak.

Table 1. Piezoelectric properties and T_C of typical KNN-based lead-free ceramics.

Materials system	Phase	d_{33}(pC/N)	k_p	T_c(℃)	Ref.
$(K_{0.44}Na_{0.52}Li_{0.04})(Nb_{0.86}Ta_{0.10}Sb_{0.04})O_3$	O-T	416	0.61	~253	7
$(K_{0.52}Na_{0.40})(Nb_{0.83}Sb_{0.09})O_3-0.08LiTaO_3$	O-T	400	0.54	~230	35
$(Na_{0.52}K_{0.40})(Nb_{0.84}Sb_{0.08})O_3$-$LiTaO_3$-$BaZrO_3$	R-T	365	0.45	~170	14
KNN-$BaZrO_3$-$LiSbO_3$	R-T	344	0.324	~176	15
(1-x)$K_{0.5}Na_{0.5}Nb_{1-x}Sb_xO_3$-$xBi_{0.5}Na_{0.5}TiO_3$	R-T	380	0.35	~276	36
(1-x)$(K_{0.42}Na_{0.58})(Nb_{0.96}Sb_{0.04})O_3$-$x(Bi_{0.5}Na_{0.5})_{0.90}Mg_{0.10}ZrO_3$	R-T	434	0.47	~244	24
(1-x)$K_{0.48}Na_{0.52}Nb_{0.95}Sb_{0.05}O_3$-$xBi_{0.5}Na_{0.5}Zr_{0.95}Ce_{0.05}O_3$	R-T	441	0.44	~215	This work

Figure 7(a) shows the thermal stability of the ceramics as a function of x, measured in the annealing

RSC Advances Accepted Manuscript

temperature range of 30~350℃ (annealing time was 30min). The d_{33} of all the ceramics decreases with the increasing annealing temperature (T_a), and most of it drops dramatically when the T_a is close to T_C. But the thermal stability of d_{33} of the ceramics with x=0.03 and 0.034 is extraordinary. Comparing with the T_C (215℃) of x=0.034, it's d_{33} gently reduce until the T_a overs 250℃. Figure 7(b) shows the $\Delta d_{33}/d_{33}$ vs. T_a curves for all the ceramics. The ceramics with x=0 and 0.02 exhibit a better thermal of d_{33} duo to the orthorhombic structure.[34,37] And the value of d_{33} of the ceramics with x=0.04 quickly decreases as T_a increases. That's partly because of lower and diffused Curie dielectric peaks. In conclusion, the ceramics with x=0.04 still exhibit a larger d_{33} value (d_{33}>330pC/N, $\Delta d_{33}/d_{33}$>75%) even if the annealing temperature reaches 250℃, which has surpassed the T_C (215℃). In this case, the annealing time is insufficient and Curie dielectric peak is in the range of 190~290℃. We think these two reasons make a larger d_{33} when T_a reached 250℃.

4.Conclusion

$(1-x)K_{0.48}Na_{0.52}Nb_{0.95}Sb_{0.05}O_3$-$xBi_{0.5}Na_{0.5}Zr_{0.95}Ce_{0.05}O_3$ ceramics were synthesized using the conventional solid-state method. The ceramics with $0.03<x<0.04$ exhibit coexistence of tetragonal phase and rhombohedral phase at room temperature. And an enhanced piezoelectric and dielectric properties is obtained in the ceramics with compositions locating in the phase boundary zone. In this work, the ceramics with x=0.034 shows the maximum value of d_{33} (~441pC/N), and a good temperature stability of piezoelectricity of this ceramics is obtained (the d_{33} is still more than 330pC/N when T_a reaches 250℃). As a result, such a material system is a promising candidate for the lead-free piezoceramics.

RSC Advances Accepted Manuscript

Acknowledgment

This work was supported by the National Natural Science Foundation of China (Nos. 51332003 and 61201064). Authors also thank Ms. Hui Wang for measuring the FE-SEM images.

RSC Advances Accepted Manuscript

References

1 B. Jaffe, R. S. Roth, and S. Marzullo, *Journal of Reseach of the National Bureaau of Standards*, 1955, **55**, 239-254.

2 B. Jaffe, Piezoelectric Ceramics, *Academic Press, India*, 1971,**Chapter 7**.

3 T. R. Shrout and S. J. Zhang, *J. Electroceram.*, 2007, **19**, 113-126.

4 J. Rödel, W. Jo, K. T. P. Seifert, E. M. Anton, *J. Am. Ceram. Soc.*, 2009, **92**, 1153-1177.

5 J. Wu, D. Xiao, J. Zhu, *Chem. Rev.*, 2015, **115**, 2559-2595

6 N. Ledermann, P. Muralt, J. Baborowski, S. Gentil, K. Mukati, M. Cantoni, A. Seifert, N. Setter, *Sensor. Actuat. A: Phys.*, 2003,**105**, 162-170.

7 Y. Saito, H. Takao, T. Tani, T. Nonoyama, K. Takatori, T. Homma, T. Nagaya, M. Nakamura, *Nature*, 2004, **432**, 84-87.

8 J. Wu, D. Xiao, Y. Wang, J. Zhu, L. Wu, and Y. Jiang, *Appl. Phys. Lett.*, 2007, **91**, 252907.

9 K. Wang and J. Li, *Adv. Funct. Mater.*, 2010,**20**, 1923-1929.

10 R. Zuo, Y. Chun, X. Fang, *Jpn. J. Appl. Phys.*, 2007,**46**, 6733-6736.

11 E.K. Akdogan, K.Kerman, M. Abazari, and A. Safari, *Appl. Phys. Lett.*, 2008, **92**, 112908.

12 R.P. Wang, H. Bando, T. Katsumata, Y. Inaguma, H. Taniguchi, and M. Itoh, *Phys. Status Solidi RRL 3.*, 2009, **5**, 142-144.

13 R. Zuo, J. Fu, D. Lv and Y. Liu, *J. Am. Ceram. Soc.*, 2010, **93**(9), 2783.

14 R. Zuo, J. Fu,*J. Am. Ceram. Soc.*, 2011, **94**(5) 1467-1470.

15 W. Liang, W. Wu, D. Xiao, J. Zhu, and J. Wu, *J. Mater. Sci.*, 2011, **46**(21), 6871-6876.

16 Q. Gou, D. Xiao, B. Wu, M. Xiao, S. Feng, D. Mazhao, J. Wu and J. Zhu, *RSC Adv.*, 2015, **5**, 30660-30666.

17 J. Wu, H. Tao, Y. Yuan, X. Lv, X. Wang and X. Lou, *RSC Adv.*, 2015, **5**,14575–14583.

18 D. Lin, K. W. Kwok, H. Tian, and H. W. L. Chan, *J. Am. Ceram. Soc.*, 2007, **90**(5), 1458-1462.

19 Y. Yuan, J. Wu, H. Tao, X. Lv, X. Wang and X. Lou, *J. Appl. Phys.*, 2015, **117**, 084103.

20 B. Sahoo, P. K. Panda, *J. Mater. Sci.*, 2007, **42**, 9684-9688.

21 D. Gao, K.W.Kwok, D. Lin, H.L.W. Chan, *J. Mater. Sci.*, 2009,**44**, 2466-2470.

22 H. Du, F. Luo, S. Qu, Z. Pei, D. Zhu, and W. Zhou, *J. Appl. Phys.*, 2007,**102**,054102 .

23 B. Malic, J. Bernard, A. Bencan and M. Kosec, *J. Eur. Ceram. Soc.*, 2008, **28**, 1191.

RSC Advances Accepted Manuscript

24 J. Wu, Y. Yang, X. Wang, D. Xiao, J. Zhu, *J. Mater. Sci: Mater Electron*, 2014, **25**, 4650-4656.

25 X. Cheng, J. Wu, X. Wang, B. Zhang, J. Zhu, D. Xiao, X.Wang, X. Lou, *Appl. Phys. Lett.*, 2013, **103**, 052906.

26 X. Wang, J. Wu, D. Xiao, J. Zhu, X. Cheng, T. Zheng, B. Zhang, X. Lou, X. Wang, *J. Am. Chem. Soc.*, 2014, **136**(7), 2905–2910.

27 C.A. Randall, N. Kim, J.P. Kucera, W. Cao, T.R. Shrout, *J. Am. Ceram. Soc.*, 1998, **81**(3), 677-688.

28 S. E. Park and T. R. Shrout, IEEE Trans. *Ultrason. Ferroelectr. Freq. Control*, 1997, **44**, 1140.

29 Z. Zhao, V. Buscaglia, M. Viviani, M. T. Buscaglia, L. Mitoseriu, A. Testino, M. Nygren, M. Johnsson and P. Nanni, *Phys. Rev. B*, 2004, **70**, 024107.

30 W. Cao and C. A. Randall, *J. Phys. Chem. Solids*, 1996, **57**(10), 1499.

31 G. Arlt and N. A. Pertsev, *J. Appl. Phys.*, 1991, **70**(4), 2283.

32 J. Wu, X. Wang, X. Cheng, T. Zheng, B. Zhang, D. Xiao, J. Zhu and X. Lou, *J. Appl. Phys.*, 2014, **115**, 114104.

33 J. Wu, Y. Wang and H. Wang, *RSC Adv.*, 2014, **4**, 64835-64842.

34 Y. Gao, J. L. Zhang, X. J. Zong, C. L. Wang and J. C. Li, *J. Appl. Phys.*, 2010,**107**, 074101.

35 R. Zuo, J. Fu and D. Lv, *J. Am. Ceram. Soc.*, 2009, **92**(1), 283-285.

36 W. Liang, Z. Wang, D. Xiao, J. Wu, W. Wu, T. Huang,J. Zhu, *Int. Ferroelectric.*, 2012, **139**, 63-74.

37 D. Lin, Z. Li, S. Zhang, Z. Xu and X. Yao, *Solid StateCommun.*, 2009, **149**, 1646 -1649.

RSC Advances Accepted Manuscript

Figure Captions

Figure 1. XRD patterns of the (1-x)$K_{0.48}Na_{0.52}Nb_{0.95}Sb_{0.05}O_3$-$x$$Bi_{0.5}Na_{0.5}Zr_{0.95}Ce_{0.05}O_3$ ceramics

Figure 2. Temperature-dependent dielectric constant of the ceramics with (a) x=0, (b) x=0.02, (c) x=0.03, (d) x=0.034, (e) x=0.04, (f) x=0.05, measured at 100 kHz and in the temperature range of -120~200℃.

Figure 3. (a) Temperature -dependent dielectric constant of the ceramics as a function of x. (b)Phase diagram of (1-x)KNNS-xBNZC ceramics.

Figure 4. Surface SEM micrographs of the ceramics with (a)x=0, (b)x=0.02, (c)x=0.034, (d)x=0.05.

Figure 5. (a) P-E curves and (b) P_r and E_C versus x of the ceramics.

Figure 6. (a) d_{33}, k_p and Q_m versus x of the ceramics. (b) ε_r and tanδ versus x of the ceramics.

Figure 7. (a) Thermal stability of d_{33} of (1-x)KNNS-xBNZC ceramics, and the insets are the thermal stability of the $d_{33}$of the ceramics with x=0.034. (b) $\Delta d_{33}/d_{33}$vs. T_a of the (1-x)KNNS-xBNZC ceramics.

RSC Advances Accepted Manuscript

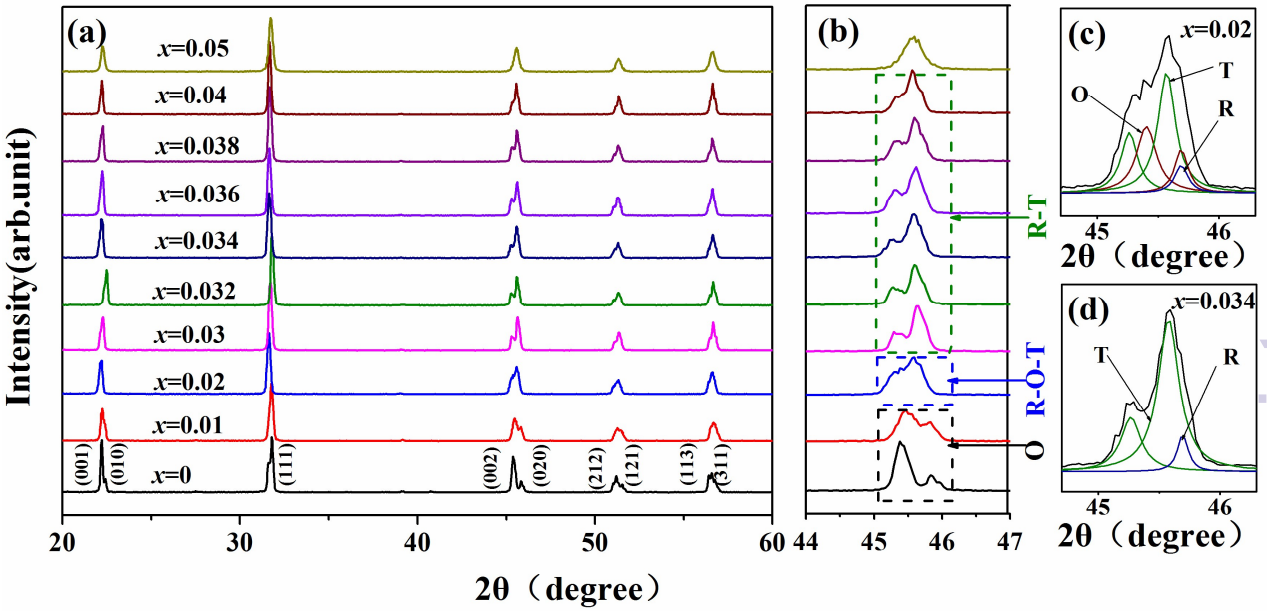

Figure 1. XRD patterns of the (1-x)$K_{0.48}Na_{0.52}Nb_{0.95}Sb_{0.05}O_3$-$xBi_{0.5}Na_{0.5}Zr_{0.95}Ce_{0.05}O_3$ ceramics

RSC Advances Accepted Manuscript

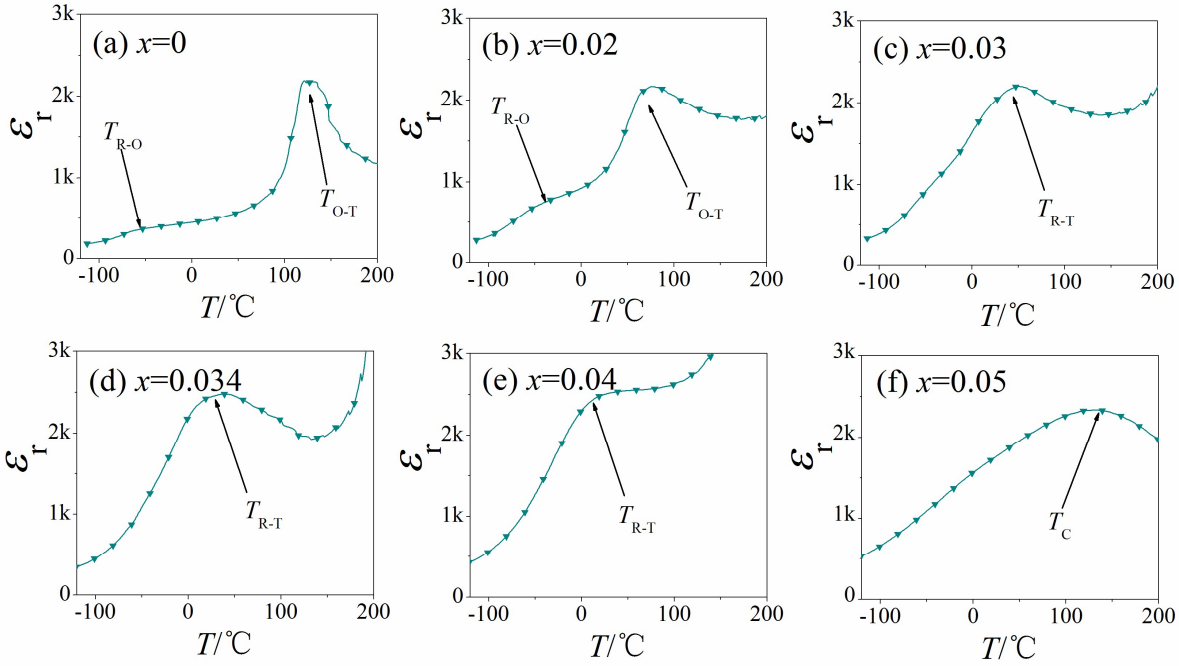

Figure 2. Temperature-dependent dielectric constant of the ceramics with (a) x=0, (b) x=0.02, (c) x=0.03, (d) x=0.034, (e) x=0.04, (f) x=0.05, measured at 100 kHz and in the temperature range of -120~200 ℃ .

RSC Advances Accepted Manuscript

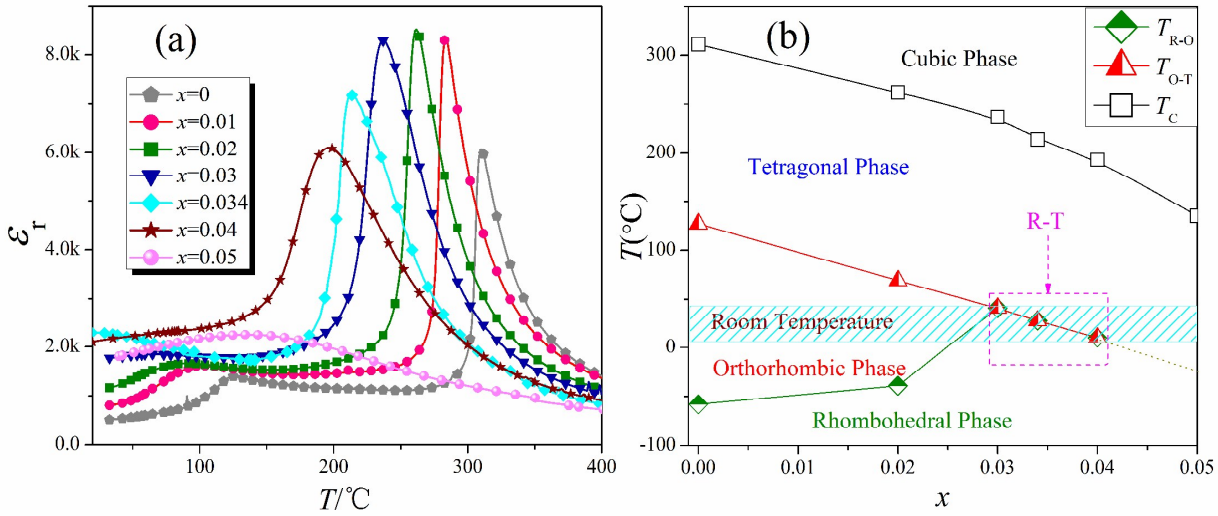

Figure 3. (a) Temperature -dependent dielectric constant of the ceramics as a function of *x*. (b)Phase diagram of (1-*x*)KNNS-*x*BNZC ceramics.

RSC Advances Accepted Manuscript

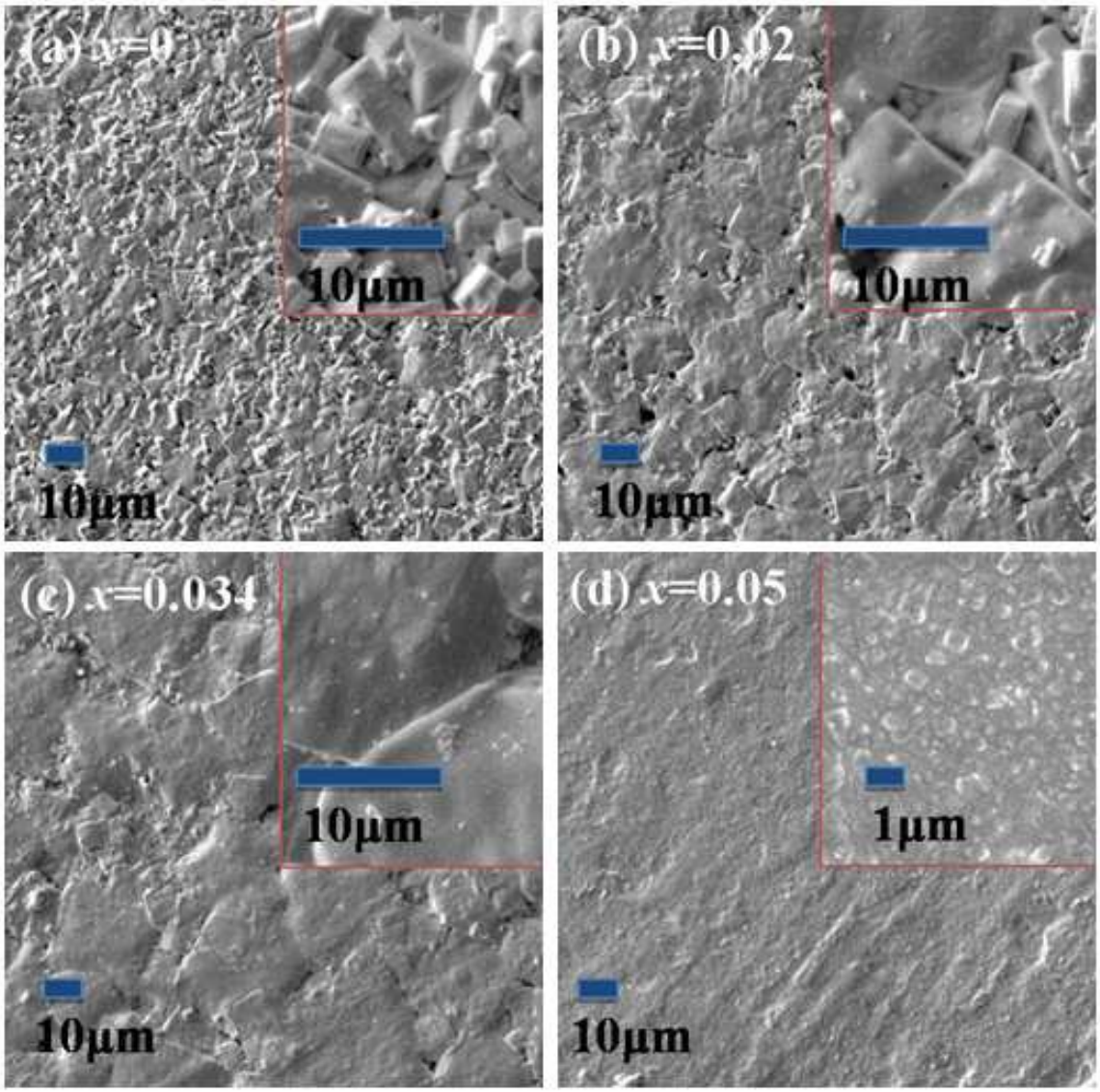

Figure 4. Surface SEM micrographs of the ceramics with (a)x=0, (b)x=0.02, (c)x=0.034, (d)x=0.05.

RSC Advances Accepted Manuscript

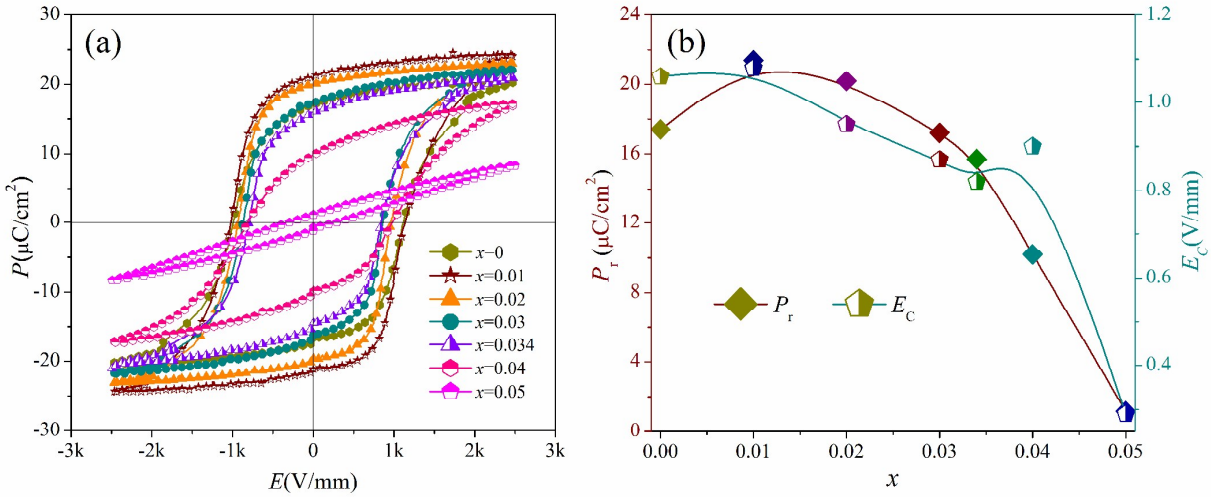

Figure5. (a) *P-E* curves and (b) P_r and E_C versus x of the ceramics.

RSC Advances Accepted Manuscript

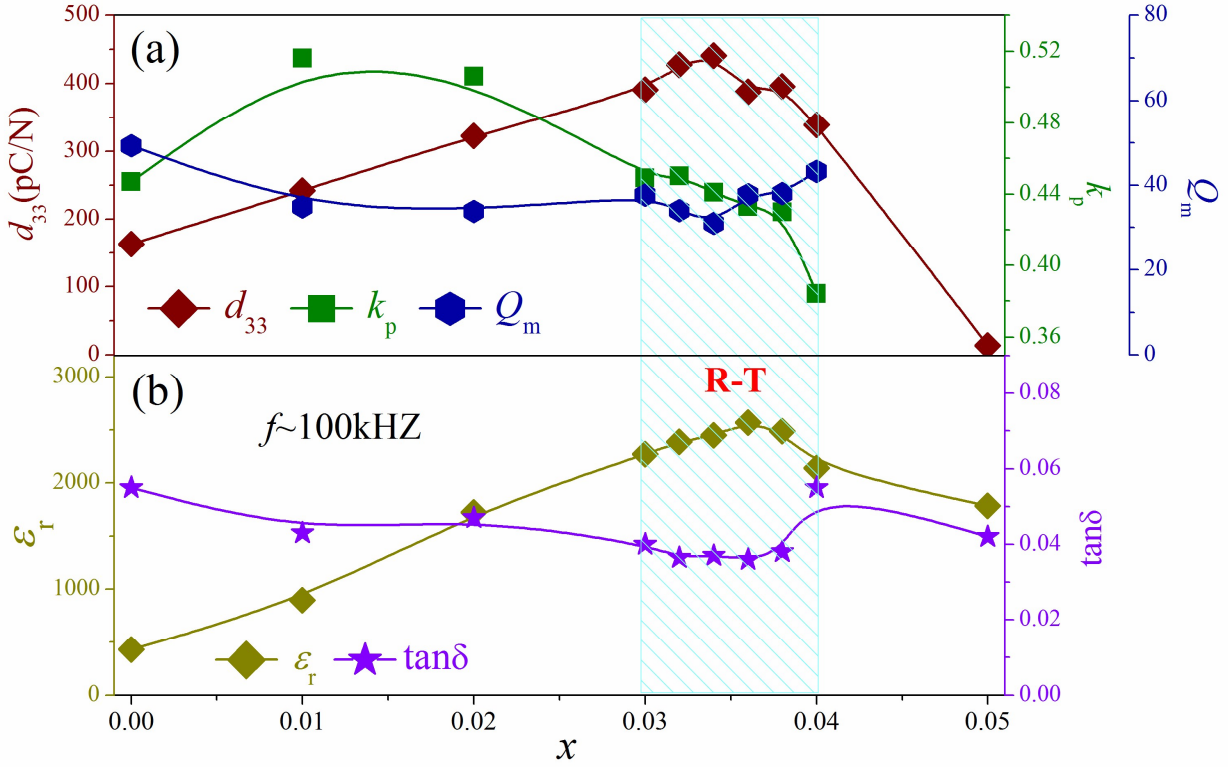

Figure 6. (a) d_{33}, k_p and Q_m versus x of the ceramics. (b) ε_r and tanδ versus x of the ceramics.

RSC Advances Accepted Manuscript

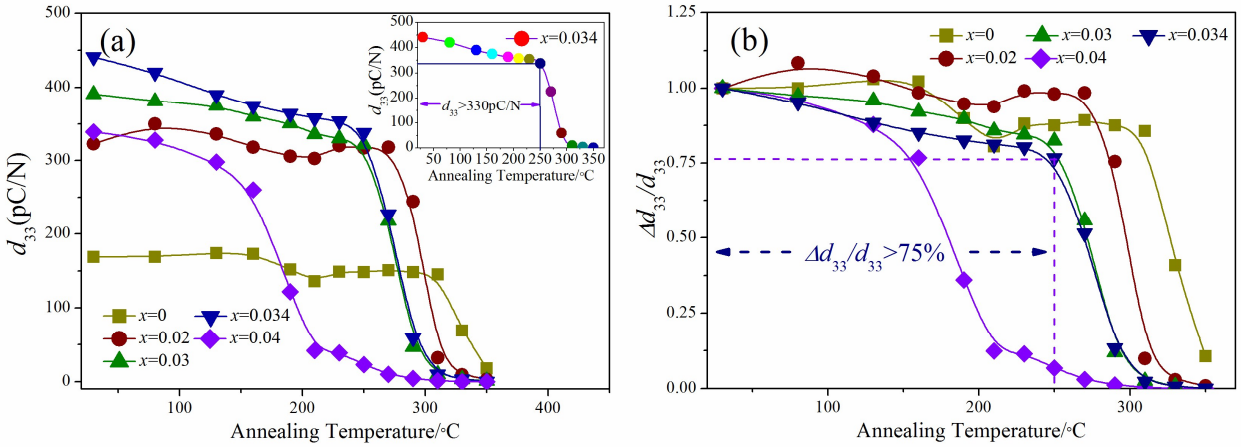

Figure 7. (a) Thermal stability of d_{33} of (1-x)KNNS-xBNZC ceramics, and the insets are the thermal stability of the $d_{33}$of the ceramics with x=0.034. (b) $\Delta d_{33}/d_{33}$vs. T_a of the (1-x)KNNS-xBNZC ceramics.

RSC Advances Accepted Manuscript